# Multiple melting temperatures in glass-forming melts

Robert Tournier, Michael I Ojovan

sustainability

MDPI

*Article*

# Multiple melting temperatures in glass-forming melts

**Robert F. Tournier [1] and Michael I. Ojovan [2,3]***

[1] UPR 3228 Centre National de la Recherche Scientifique, Laboratoire National des Champs Magnétiques Intenses, European Magnetic Field Laboratory, Institut National des Sciences Appliquées de Toulouse, Université Grenoble Alpes, F-31400 Toulouse, France ; robert.tournier@lncmi.cnrs.fr
[2] Department of Materials, Imperial College London, London SW7 2AZ, UK; m.ojovan@imperial.ac.uk
[2] Department of Radiochemistry, Lomonosov Moscow State University, 119991 Moscow, Russia
* Correspondence: m.ojovan@imperial.ac.uk

**Abstract:** All materials are vitrified by fast quenching even monoatomic substances. Second melting temperatures accompanied by weak exothermic or endothermic heat are often observed at $T_{n+}$ after remelting them above the equilibrium thermodynamic melting transition at $T_m$. These temperatures $T_{n+}$ are due to the breaking of bonds (configurons) or antibonds depending on the thermal history which is explained by using a non-classical nucleation equation. Their multiple existence in monoatomic elements is now demonstrated by molecular dynamics simulations and still predicted. Proposed equations show that crystallization enthalpy is reduced at the temperature $T_x$ due to new vitrification of non-crystallized parts and their melting at $T_{n+}$. These glassy parts being equal above $T_x$ to singular values or to their sum are melted at various temperatures $T_{n+}$ and attains 100% in $Cu_{46}Zr_{46}Al_8$ and 86.7% in bismuth. These first-order transitions at $T_{n+}$ are either reversible or irreversible depending on the formation of superatoms either solid or liquid.

**Keywords:** metallic glasses; melting temperatures; liquid-liquid transitions, chemical bonds; vitrification, crystallization, first order transitions

**Citation:** Tournier R.F., F.; Ojovan M.I. Title. *Sustainability* **2022**, *14*, x. https://doi.org/10.3390/xxxxx

Academic Editor: Firstname Lastname

Received: date
Accepted: date
Published: date



## 1. Introduction

Liquid-liquid phase transitions occur in glass-forming melts below and above $T_m$, the equilibrium thermodynamic melting transition of crystals. These transitions are driven by density separation of two liquid states existing in all supercooled and overheated materials including pure elements in which two liquid phases of the same composition coexist [1-15]. Denser glassy phases are built by vapor deposition below the glass transition temperature $T_g$ leading to higher glass transition temperatures and first-order transitions toward liquid states [16-19]. Glacial phases with higher values of $T_g$ result from first-order transitions between $T_g$ and $T_m$ [20-25]. Denser phases called G-Phases are obtained in liquid elements by numerical simulations at very high heating rates, leading to second melting temperatures far above $T_m$ [26-29]. Glass-forming melts undergo liquid-liquid transitions with endothermic or exothermic latent heats at nucleation temperatures $T_{n+}$ higher than $T_m$ [30-36]. First-order transitions are observed at temperatures $T_{n+}$ above $T_m$ with nuclear magnetic resonance by cooling a homogeneous liquid, followed by homogeneous nucleation of growth nuclei below $T_{n+}$ leading to melt crystallization [37,38]. Multiple liquid-liquid transitions were observed at low heating rates in bismuth [39.40] and glass-forming melts of Cu-Zr-Al [41]. It is the purpose of this publication to relate the various glass phases to melting transitions above Tm following proposals of H. Tanaka [15,42].

Liquid–liquid structure transition plays an important role in the final microstructure and the properties of solid alloys [43]. Solidifying $Bi_2Te_3$ alloys after melting above $T_{n+}$ followed by various cooling rates refined the microstructure and increased the hardness with cooling rate [44,45]. Solidifying magnetic melts after overheating below $T_{n+}$ in high magnetic fields built textured congruent and non-congruent substances [46], crystals or

even permanent magnets with particle easy-magnetization axis oriented along the magnetic field due to the presence of growth nuclei in melts above $T_m$ [47]. The classical nucleation equation cannot explain such nucleation phenomena [48,49].

A non-classical nucleation equation involving two liquid states was built by adding an enthalpy contribution $\varepsilon H_m$, with $\varepsilon$ depending on $\theta^2 = (T-T_m)^2/T_m^2$ and being a fraction of the crystal melting heat $H_m$ to complete the Gibbs free energy of nuclei above and below $T_m$ [50]. The undercooling rate of liquid elements were predicted leading to an average minimum value of $\varepsilon = 0.217$ for $\theta = 0$ due to the Lindemann coefficient at $T_m$ [51]. The nucleation equations of liquids 1 and 2 were used to successfully predict the specific heat jump at the glass transition temperature $T_g$, the VFT temperatures of fragile liquids above $T_m/3$ [52-54] and the first temperature $T_{n+}$ [55]. The nature of surviving entities are superclusters (superatoms), melted by liquid homogeneous nucleation instead of surface melting [56,57].

The enthalpy and entropy variations of supercooled water at $T_{LL} = 228.5$ K [58,59] during the first cooling were predicted [60]. The formation below $T_g$ of a glacial phase called Phase 3, having an enthalpy equal to the difference between those of liquids 1 and 2, explained why the transition at $T_{LL}$ disappears during the first heating. The theoretical first-order transitions of Phase 3 under pressure reproduced those found by Speedy and Angell [61]. The phase diagram of water confined into carbon nanotubes was similar to that predicted by numerical simulations [62,63].

The thermodynamic properties of glass-forming melts are easy to predict when $T_g$ and $T_m$ are known. The singular enthalpy values of Phase 3 are zero and those calculated at $T = T_m$, $T_g$, $T_{om}$, the VFT temperatures of liquids 1 and 2 and the first temperature $T_{n+}$. The nucleation equations of glacial phases used these singular enthalpies as latent heats to fix the entropy-driven transition temperatures [64,65] of triphenyl phosphite [22,25], D-mannitol [24], *n*-butanol [23,66,67], and $Zr_{41.2}Ti_{13.8}Cu_{12.5}Ni_{10}Be_{22.5}$ [35,36]. The stable and ultrastable glasses formed by vapor deposition had enthalpies equal to singular values and their transition temperatures at $T_g$ are driven by them. Other melts had also enthalpy-driven transitions such as $Ti_{34}Zr_{11}Cu_{47}Ni_8$ [68], and $Co_{81.5}B_{18.5}$ [43] in agreement with the predictions [65]. A critical supercooling and overheating rate $\Delta T/T_m = 0.198$ of liquid elements was predicted in agreement with experiments on Sn droplets [69].

Phase 3 formation has for origin a second-order phase transition associated with critical exponents due to bonds breaking (configurons formation) when a glass is heated through $T_g$ [70-75]. The Gibbs free energy of configurons disappears at $T_{n+}$ instead of $T_g$ [62,76,77]. The debate about the absence and the presence of phase transition at $T_g$ is probably solved by these considerations.

The non-classical nucleation model predicted the G-phase formation in liquid elements via first-order transitions, and the second melting temperatures observed by molecular dynamics simulations at very high heating rates [78,79].

The question of their observation at low heating rates was raised, considering that the crystallization enthalpy of these elements would be reduced and recovered via liquid-liquid transitions occurring above $T_m$. The singular values of the latent heats in all glass-forming melts could correspond to percolation thresholds at various temperatures.

The coexistence of glassy phases with crystals is known and viewed as being due to phase separation after annealing near $T_x$, the crystallization temperature of glass-forming melts. This coexistence could result in fact from the presence of a glassy fraction in nanocrystallized materials having a glass transition temperature $T_g$ higher than $T_m$ as already shown for liquid elements [79].

This paper is devoted to the second vitrification of melt fractions at temperatures $T_x$ coexisting with crystals formation and predictions of multiple melting temperatures $T_{n+}$ of this glassy fraction above Tm from singular enthalpies of glass-forming melts.

## 2. The homogenous nucleation of two glassy states

### *2.1. The bulk glassy state below $T_g$*

The Gibbs free energy change for a nucleus formation in a melt is given by (1) [ (50)]:

$$\Delta G_{ls} = (\theta - \varepsilon_{ls})\,\Delta H_m/V_m \times 4\pi R^3/3 + 4\pi R^2\sigma_{ls}, \quad (1)$$

where R is the nucleus radius and following Turnbull [48], $\sigma_{ls}$ its surface energy, given by (2), θ the reduced temperature $(T-T_m)/T_m$, $\Delta H_m$ the melting enthalpy at $T_m$, and $V_m$ the molar volume:

$$\sigma_{ls}(V_m/N_A)^{-1/3} = \alpha_{ls}\,\Delta H_m/V_m, \quad (2)$$

A complementary enthalpy $\varepsilon_{ls}\times\Delta H_m/V_m$ is introduced, authorizing the presence of growth nuclei above and below $T_m$ with $\varepsilon_{ls}$ being positive or negative above $T_m$ depending on its increase or decrease with θ. In previous works, $\varepsilon_{ls}$ was only positive [50,52,54,80]. The discovery of positive or negative enthalpy above $T_m$ related to the presence of anti-bonds or bonds sets this new rule [77]. The classical nucleation equation is obtained for $\varepsilon_{ls}= 0$ and leads to a homogeneous liquid above $T_m$.

The critical thermally activated energy barrier $\Delta G^*_{ls}/k_BT$ is calculated in (3) assuming $d\varepsilon_{ls}/dR = 0$:

$$\frac{\Delta G^*_{ls}}{k_BT} = \frac{16\pi\Delta S_m\,\alpha^3_{ls}}{3N_Ak_B(1+\theta)(\theta-\varepsilon_{ls})^2}, \quad (3)$$

where $\Delta S_m$ is the melting entropy [48,50,54,81]. This critical parameter is no longer infinite at the melting temperature $T_m$ because $\varepsilon_{ls}$ is not equal to zero. This event now occurs above $T_m$ for $\theta= \varepsilon_{ls}$. The nucleation rate $J = K_v \exp(-\Delta G^*_{ls}/k_BT)$ is equal to 1 when (4) is respected:

$$\Delta G^*_{ls}/k_B\,T = \ln(K_v), \quad (4)$$

The surface energy coefficient $\alpha_{ls}$ in (2) is determined from (3,4) and equal to (5):

$$\alpha^3_{ls} = \frac{3N_Ak_B\,(1+\theta)(\theta-\varepsilon_{ls})^2}{16\pi\Delta S_m}\ln(K_v), \quad (5)$$

The nucleation temperatures $\theta_{n-}$ and $\theta_{n+}$ obtained for $d\alpha^3_{ls}/d\theta = 0$ obey (6):

$$d\alpha^3_{ls}/d\theta \sim (\theta_{n+} - \varepsilon_{ls})(3\theta_{n-} + 2 - \varepsilon_{ls}) = 0, \quad (6)$$

There are two families of nucleation temperatures: $\theta_{n-}= (\varepsilon_{ls}-2)/3$ far below $T_m$ and $\theta_{n+}= \varepsilon_{ls}$ above $T_m$. In addition to the nucleation temperatures $T_{n-}$ below $T_m$, the existence of a homogenous nucleation temperature $T_{n+}$ above $T_m$ is confirmed by many experiments, observing the undercooling versus the overheating rates of liquid elements, and glass-forming melts [43,69,82-85]. This nucleation temperature has for consequence, the existence of a second melting temperature $T_{n+}$ of growth nuclei above $T_m$ and of their homogeneous nucleation at temperatures weaker than $\theta_{n+}$ as shown in several publications [30-39,86-89].

The coefficient $\varepsilon_{ls}$ of the initial liquid state called liquid 1 is a quadratic function of θ in (7) [50] for $\varepsilon_{ls}> 0$ above $T_m$ in (1):

$$\varepsilon_{ls} = \varepsilon_{ls0}(1 - \theta^2/\theta^2_{0m}), \quad (7)$$

where $\theta_{0m}$ is the Vogel-Fulcher-Tammann (VFT) reduced temperature leading to $\varepsilon_{ls}= 0$ for $\theta = \theta_{0m}$, and the VFT temperature $T_{0m}$ of many fragile liquids being equal to ≅ 0.77 $T_g$. This quasi-universal value is known for numerous fragile liquids including atactic polymers [90,91].

New liquid states are obtained for $\theta= \theta_{n+}= \varepsilon_{ls}$ and $\theta= \theta_{n-}= (\varepsilon_{ls}-2)/3$ where $\varepsilon_{ls}$ is given in (7). The reduced nucleation temperatures $\theta_{n-}$ are solutions of the quadratic equation (8):

$$\varepsilon_{ls0}\theta^2_{n-}/\theta^2_{0m} + 3\theta_{n-} + 2 - \varepsilon_{ls0} - \Delta\varepsilon = 0, \text{ or } \varepsilon_{ls}(\theta = 0) = (3\theta_{n-} + 2 - \Delta\varepsilon)/(1 - \frac{\theta^2_{n-}}{\theta^2_{0m}}) \quad (8)$$

where Δε is an enthalpy-coefficient change, which can induce a first-order transition [55].

There is a minimum value of $\varepsilon_{ls0}$ plotted as a function of $\theta_{0m}$ using (8) for $\Delta\varepsilon = 0$ and $\theta_{n-} = (\varepsilon_{ls}-2)/3$, determining the relation (9) between $\theta^2_{0m}$ and $\varepsilon_{ls0}$ for which the two solutions of (8) are equal in fragile liquids [52,53]. These values define the temperature where the surface energy is minimum and $\theta^2_{0m}$ and $\varepsilon_{ls0}$ obey (9) and (10):

$$\theta^2_{0m} = \frac{8}{9}\varepsilon_{ls0} - \frac{4}{9}\varepsilon^2_{ls0}, \quad (9)$$

$$\varepsilon_{ls}(\theta = 0) = \varepsilon_{ls0} = 1.5\theta_{n-} + 2 = a\theta_g + 2, \quad (10)$$

Eq. (9) leads to $T_{0m} = 0.769\times T_g$ for a= 1 in agreement with many experimental values [52].

All melts and even liquid elements undergo, in addition, a bulk glass transition because another liquid state called liquid 2 exists characterized by an enthalpy coefficient $\varepsilon_{gs}$ given by (11) inducing an enthalpy change from that of liquid 1 at the thermodynamic transition at $\theta_g$ [53,54,80]:

$$\varepsilon_{gs} = \varepsilon_{gs0}(1 - \theta^2/\theta^2_{0g}) - \Delta\varepsilon, \quad (11)$$

where $\theta_{0g}{}^2$ and $\varepsilon_{gs0}$ obey (12,13) for $\varepsilon_{ls} > 0$ and $\Delta\varepsilon$ is zero at the glass transition:

$$\theta^2_{0g} = \frac{8}{9}\varepsilon_{gs0} - \frac{4}{9}\varepsilon^2_{gs0}, \quad (12)$$

$$\varepsilon_{gs}(\theta = 0) = \varepsilon_{gs0} = 1.5\theta_{n-} + 2 = 1.5\theta_g + 2, \quad (13)$$

The reduced nucleation temperatures $\theta_{n-}$ are solutions of the quadratic equation (14):

$$\varepsilon_{g0}\theta^2_{n-}/\theta^2_{0g} + 3\theta_{n-} + 2 - \varepsilon_{gs0} - \Delta\varepsilon = 0, \text{ or } \varepsilon_{gs}(\theta = 0) = (3\theta_{n-} + 2 - \Delta\varepsilon)/(1 - \frac{\theta^2_{n-}}{\theta^2_{0g}}) \quad (14)$$

where $\Delta\varepsilon$ is the enthalpy-coefficient change inducing a first-order transition [55,66]. Eqs (8) and (14) lead to the same nucleation temperature $T_{n-} = T_g$ for the same coefficient $\Delta\varepsilon$ in fragile liquids.

### *2.2. The glassy state of Phase 3 up to the melting temperature $T_{n+}$ above $T_m$*

The difference $\Delta\varepsilon_{lg}$ in (15) between the coefficients $\varepsilon_{ls}$ and $\varepsilon_{gs}$ determines the Phase 3 and the configuron enthalpies when the quenched liquid has escaped crystallization [58,59,76]:

$$\Delta\varepsilon_{lg}(\theta) = [\varepsilon_{ls} - \varepsilon_{gs}] = [\varepsilon_{ls0} - \varepsilon_{gs0} - \Delta\varepsilon - \theta^2\left(\varepsilon_{ls0}/\theta^2_{0m} - \varepsilon_{gs0}/\theta^2_{0g}\right)], \quad (15)$$

The assumption of a= 1 in (10) defining the value of $T_{0m}$ in (9) is the unique value for which the activation energies $B_1RT/(T-T_{0m})$ and $B_2RT/(T-T_{0g})$ of liquids 1 and 2 are equal at $T_g$ leading to an activation energy equal to zero for Phase 3 [76].

When the enthalpy coefficients $\varepsilon_{ls}$ ($\theta$) and $\varepsilon_{gs}$ ($\theta$) are negative in (1), the phase 3 enthalpy coefficient $\Delta\varepsilon_{lg}$ ($\theta$) becomes equal to (16):

$$\Delta\varepsilon_{lg}(\theta) = -[\varepsilon_{ls} - \varepsilon_{gs}] = -[\varepsilon_{ls0} - \varepsilon_{gs0} - \Delta\varepsilon - \theta^2\left(\varepsilon_{ls0}/\theta^2_{0m} - \varepsilon_{gs0}/\theta^2_{0g}\right)], \quad (16)$$

It increases with $\theta$ in (15) or decreases in (16) because of its dependence on the thermal history and disappears at $T_{n+}$. Two reduced glass transition temperatures $\theta_g$ and $-\theta_g$ exist. Another analogous equation leading to $\Delta\varepsilon_{lg}$ ($\theta$) given in (16) can be determined using the new coefficients $\varepsilon_{ls0}$ and $\varepsilon_{gs0}$ in (10,13) obtained by changing $\theta_g$ in $-\theta_g$ and $\theta^2_{0m}$, $\theta^2_{0g}$ deduced from (9,12) using these new values of $\varepsilon_{ls0}$ and $\varepsilon_{gs0}$.

These new considerations show the existence of a glassy state of a melt fraction disappearing at the virtual transition temperature $T'_g = 2T_m - T_g$ governing the thermodynamics of all Phases 3 including those nucleated by first-order transitions. This phenomenon

of double glass state occurs because all glass-forming melts heated from their glass state are composites containing an ordered fraction of percolating bonds or antibonds (15 ± 1 % minimum) and a homogeneous liquid (85 % maximum) [62,76,77]. The first glass transition temperature, observed at $T_g$ below $T_m$ by heating, corresponds to the percolation of configurons in the bulk liquid while the second transition only due to Phase 3 disappears at $T_{n+}$ far above $T_m$. The partial glass state is preserved up to the nucleation temperature $\theta_{n+}= \Delta\varepsilon_{lg}$ ($\theta_g$) because the ordered fraction remains equal to the percolation threshold observed at $\theta_g$ below $T_m$. The melt transformations at $\theta_{n+}$ are sharp and only observable below the virtual glass transition occurring at $\theta'_g = -\theta_g$. Note that the two VFT temperatures above $T_m$ corresponding to this virtual glass transition are also virtual because $\theta^2_{0m}$ and $\theta^2_{0g}$ are negative in this case.

## 3. Reduction of the crystallization enthalpy at the crystallization temperature $T_x$

The enthalpy recovery during heating is endothermic at $T_{n+}$ for bonds and exothermic for antibonds breaking [77]. The total melting enthalpy H depends on the reduced temperature $\theta_{n+}$ because this homogeneous nucleation temperature $T_{n+}$ occurs above $T_m$ with the enthalpy change $\Delta\varepsilon_{lg}$ ($\theta_{n+}$) = $\pm\theta_{n+}$ [1] for $\theta_{n+} < -\theta_g$.

Heating from the glass state below $T_g$ can induce, at the same time, a first-order transition at $T_x$, toward crystallization and nucleation of a new glassy state of Phase 3 with a latent heat $-\Delta\varepsilon H_m$ and a new glass transition temperature $T'_g = 2T_m - T_g$. The reduced temperature $\theta_x$ is given by Eq. (14) with $\Delta\varepsilon$ equal to singular values of the enthalpy coefficient $\Delta\varepsilon_{lg}$ of Phase 3. These singular values are zero, $\Delta\varepsilon_{lg0}/2$, $\theta_{n+}$, $\Delta\varepsilon_{lg0}$, $-\Delta\varepsilon_{lg}$ ($\theta_{0m}$) or the sum of several singular values as observed in liquid elements and as expected from hidden thresholds of configurons [78,79]. The crystallization enthalpy at $T_x$ of the liquid phase coexisting with glassy Phase 3 is given by (18):

$$H_{cr} = H_m(-1 + \Delta\varepsilon), \quad (18)$$

The melting heat $H_{3m}$ of each Phase 3 depends on its singular value and its contribution to $\Delta\varepsilon$ at $T_x$. This melting, depending on the heating rate, occurs at various reduced temperatures $\theta_{n+}$ defined for each singular value of $\Delta\varepsilon$ or is associated with other singular values or leads to a unique melting temperature $\theta_{n+}= \Delta\varepsilon$:

$$H_{3m} = H_m \times \theta_{n+}, \quad (19)$$

The temperature $T_x$ separates the two domains of glassy phases between $T_g$ and $T_{n+}$. Below $T_g = T_x$, the bulk glassy domain takes place after the fist-order transition at $T_x$ while the glassy fractions induced at $T_x$ disappear at $T_{n+}$ without attaining the virtual glass transition temperature $T'_g$ equal to ($2T_m - T_g$). The glass enthalpy disappears at $T_{n+} < T'_g$ by heating from $-\Delta\varepsilon H_m$ to 0 giving rise to homogeneous liquid.

## 4. 4- Gleaning information in published works to predict the crystallized fraction from the knowledge of $T_x$ or melting temperatures of various Phases 3 above $T_m$

### *4.1. Three melting temperatures of bismuth were observed above $T_m$ in two different experiments*

DSC measurements of bismuth with a heating rate of 0.083 K/s showed two endothermic transitions at $T_{1n+}$= 504.9 °C (778 K) and $T_{2n+}$= 511.5 K (784.6 K) above the melting temperature $T_m$= 544.5 K as shown in Figure 1 [39]. A third transition were observed with the density at $T_{3n+}$ = 1013 K in another experiment in the absence of transformations at $T_{1n+}$ and $T_{2n+}$ [40].

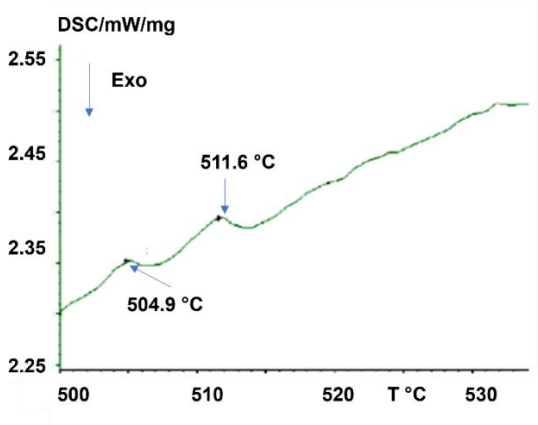


**Figure 1.** Experimental results for DSC of bismuth. Reproduced with permission from [ (39)] Figure 2a. Copyright 2004 Elsevier.

With the model already developed for other liquid elements [79], these temperatures are used to calculate a Bi Lindemann coefficient equal to 0.09119 in good agreement with the value 0.095 recently found [92]. The glass transition temperature is predicted at $T_g$= 203.5 K and the singular enthalpy coefficients $\Delta\varepsilon$ are $\Delta\varepsilon_{lg0}$= 0.1907, $-\Delta\varepsilon_{lg}$ ($\theta_g$) = 0.094065, $-\Delta\varepsilon_{lg}$ ($\theta_{0m}$= -2/3) = 0.10594 and $-\Delta\varepsilon_{lg}$ ($\theta$= -1) = 0.238375. The experimental coefficients $\Delta\varepsilon$ giving rise to $\theta_{1n+}$= 778/544.5 -1= 0.429 and $\theta_{2n+}$= 784.6/544.5 -1= 0.44096 are equal to the theoretical ones 0.1907+0.238375 = 0.429075 and 0.094065+0.10594+0.238375= 0.43838 respectively. The total glassy fraction melted at the two temperatures $T_{n+}$ represent 86.7% while the crystallized fraction melted at $T_m$ would be 13.3%. The transition at $T_{3n+}$ is expected at $\theta_{3n+}$ = 0.8675 ($T_{3n+}$= 1.8675$T_m$) corresponding to 1016 K in the absence of transitions at $T_{1n+}$ and $T_{2n+}$ in agreement with the second experiment. The formation of distinct glassy phases with singular enthalpies at $T_x$ depends on the heating rate.

*4.2. Crystallization enthalpy reduction of $Pd_{40}Ni_{40}P_{20}$ at the temperature $T_x$ after quenching and various annealing of the same duration at lower temperatures*

The bulk melting temperature is $T_m$ = 870 K; the glass transition temperature of ribbons is $T_g$= 575 K ($\theta_g$ = -0.33909) and the virtual glass transition temperature $T'_g$= 2$T_m$-$T_g$ = 1165 K ($\theta_{n+}$ = 0.33909). The first-order transition at $T_x$ is unique and shown in Figure 2 [93]. An endothermic transition was observed at $T_{1n+}$= 984 K above $T_m$ [94]. The enthalpy coefficients are calculated using (9,10,12,13), $\theta_g$ = -0.33908 and a= 1. Liquids 1, 2, and 3 obey (20,21,22) respectively:

$$\varepsilon_{ls} = 1.66092(1 - \theta^2/0.250305), \quad (20)$$

$$\varepsilon_{gs} = 1.49138(1 - \theta^2/0.33713), \quad (21)$$

$$\Delta\varepsilon_{lg}(\theta) = [\varepsilon_{ls} - \varepsilon_{gs}] = [0.16954 - \Delta\varepsilon - 2.2118 \times \theta^2]. \quad (22)$$

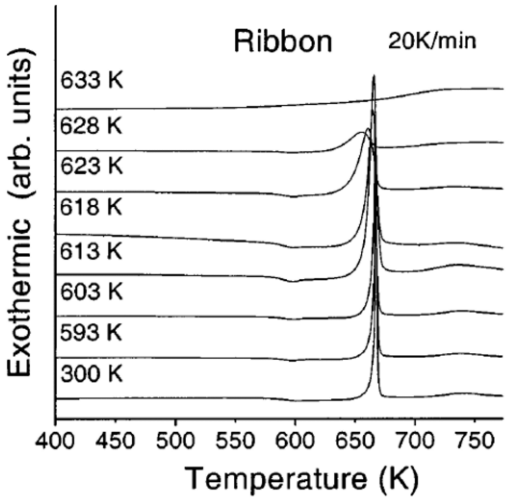


**Figure 2.** The DSC traces of the as-prepared $Pd_{40}Ni_{40}P_{20}$ ribbon glass reproduced with permission from [93]. Samples annealed at different temperatures in the supercooled liquid region for 30 minutes and heated from 300 K at a heating rate of 20 K/min under a flow of purified argon. Copyright 2002 AIP Publishing.

The first-order transition at $T_x$= 639 K, driven by the entropy of Phase 3, counted from its formation temperature at 529.36 K, being equal to ($\Delta\varepsilon_{lg}$-0.21614) ×$H_m/T_x$, leads to a singular enthalpy of Phase 3 equal to -0.21614×$H_m$ [64,65]. The singular enthalpy coefficients, $\Delta\varepsilon=\theta_{n+}$ are: 0, $\Delta\varepsilon_{lg0}/2$ = 0.08477, 0.13197, $\Delta\varepsilon_{lg0}$ = 0.16984, -$\Delta\varepsilon_{lg}$ ($\theta_{0m}$) = 0.38409 and the sums 0.13137+0.08477= 0.21614 and 0.38409 + 0.16954 + 0.13197 + 0.08477= 0.76977. The crystallization enthalpies roughly correspond to these singular values of $\theta_{n+}$ as shown in Figure 3 with (18) respected. Additional melting temperatures are also predicted above $T_m$. The transition at $T_x$ is sharp in Figure 2 up to $T_a$= 618 K ($\Delta\varepsilon = \theta_{n+}$= 0.16954) and more broaden above. The transition at $\theta_{n+}$ above $T_m$ is expected to be observable up to $\theta'_g$= 0.33909= 2$T_m$-$T_g$. Too-high ~~Higher~~ values of $\Delta\varepsilon$ above $\theta'_g$ led to higher fractions of crystalline phase.

The first-order transition at $T_x$ is expected to induce a glassy fraction of 33.909 % which melts at $T_{n+}$= 0.33909. The crystallization enthalpy, after various annealing, is strongly reduced because it roughly cumulates several singular values of $\Delta\varepsilon$ below $\theta_{n+}$= 1 when the annealing temperature $T_a$ passes 623 K.

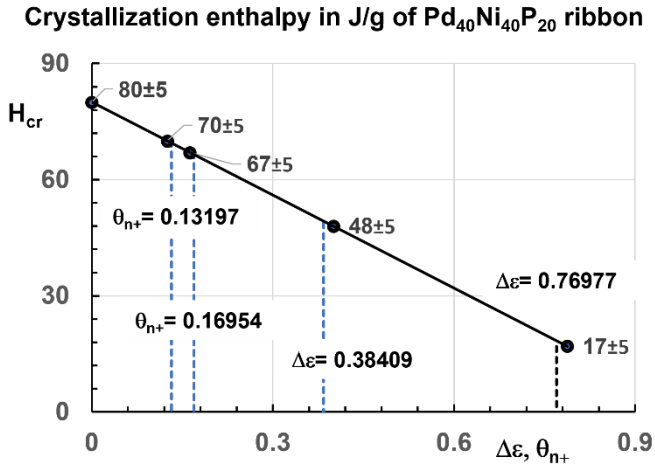


**Figure 3.** Crystallization enthalpies $H_{cr}$ in J/g, measured in $Pd_{40}Ni_{40}P_{20}$ ribbon by [93] versus the glassy Phase 3 melting at $\theta_{n+}$ and calculated with (18). The singular enthalpy coefficients are deduced from (27-29). The experimental uncertainty on $H_{cr}$ is ±5 J/g. Crystallizations for $\Delta\varepsilon$= 0.76977 and 0.38409 occurring at $T_x$. Values of $H_{cr}$ taken from [93] Figure 3.

*4.3. Melting temperatures of $Co_{76}Sn_{24}$ above $T_m$= 1392 K*

The melting temperature of $Co_{76}Sn_{24}$ is $T_m$ = 1382 K. The first temperature $T_{1n+}$ of this alloy is observed at 1583 ±10 K accompanied by an endothermic enthalpy [83,95]. Using (23) [55], the glass transition temperature $T_g$ is predicted as being equal to 866.9 K ($\theta_g$= -0.37275) for $T_{n+}$= 1581.6 K ($\theta_{n+}$= 0.14441) while the virtual glass transition is ($2T_m$-$T_g$) = 1897.14 K:

$$\theta_{n+} = -0.38742 \times \theta_g. \quad (23)$$

The enthalpy coefficients are calculated using (9,10,12,13) and a= 1. Liquids 1, 2, and 3 obey (24,25,26) respectively:

$$\varepsilon_{ls} = 1.62725(1 - \theta^2/0.26958), \quad (24)$$

$$\varepsilon_{gs} = 1.44088(1 - \theta^2/0.35806), \quad (25)$$

$$\Delta\varepsilon_{lg}(\theta) = [\varepsilon_{ls} - \varepsilon_{gs}] = [0.18637 - 2.0121 \times \theta^2]. \quad (26)$$

The singular values of the enthalpy coefficient $\Delta\varepsilon_{lg}$ ($\theta$) are: $\Delta\varepsilon_{lg}$ ($\theta_g$) = -$\Delta\varepsilon_{lg0}$ /2= -0.18637/2 for a stable glass, $\Delta\varepsilon_{lg}$ ($\theta_{1n+}$) = -0.14441, $\Delta\varepsilon_{lg0}$= -0.18637 for an ultra-stable glass, $\Delta\varepsilon_{lg}$ ($\theta_{0m}$) = -0.35605. Two first-order transition temperatures were observed at $T_{n-}$= 1129 K and 1263 K by supercooling [83,95]. They are predicted using (14) with the singular values of $\Delta\varepsilon$= $\theta_{n+}$= 0.14441 and 0.33078= 0.14441+0.18637. The transition for $\Delta\varepsilon_{lg}$= -0.35605 does not exist because it would lead to a second melting temperature higher than the glass transition $T'_g$= 1897.14 K.

The equations (27,28,29) used to predict Phase 3 enthalpy decreasing with temperature are determined with $\theta_g$= 0.37275 ($T_g$= 1897.14 K) and (9,10,12,13).

$$\varepsilon_{ls} = 2.37275(1 + \theta^2/0.34266), \quad (27)$$

$$\varepsilon_{gs} = 2.49617(1 - \theta^2/0.55046), \quad (28)$$

$$\Delta\varepsilon_{lg}(\theta) = [\varepsilon_{ls} - \varepsilon_{gs}] = [-0.18637 + 2.0121 \times \theta^2]. \quad (29)$$

Lines 1 and 2 determined by (26) and (29) in Figure 5 are obtained by heating from various glassy states depending on thermal history and heating rate and leading to exothermic or endothermic transitions at $T_{1n+}$= 1581.6 K. An endothermic transition was observed at $T_{1n+}$ [95].

The transformation at $T_x$ of Phase 3 by heating from the glassy state is predicted using (14) with $\Delta\varepsilon$= 0.33078= 0.14441+0.1837, $\varepsilon_{ls0}$= 1.44088, and $\theta_{0g}^2$= 0.35806 and leads to a negative enthalpy coefficient equal to -0.33078 as shown in Figure 4. The enthalpy of Phase 3, 0.33078×$H_m$, would be recovered at the second melting temperatures $T_{n+}$= 1581.6 K ($\theta_{n+}$= 0.14441) and 1639.6 K ($\theta_{n+}$= 0.18637). The melting enthalpy of the crystallized part would be (1-0.33078) $H_m$ = 0.66933×$H_m$ while the crystallization enthalpy would be -0.66933×$H_m$.

The temperatures $T_x$ would separate two domains of glassy states. The melt would be fully glassy below $T_x$ after transition at $T_x$ and partially glassy from $T_x$ to $T_{n+}$. The glassy fractions of the melt would be 33.078% from $T_x$ to 1581.6 K and 18.637% from 1581.6 to 1639.6 K.

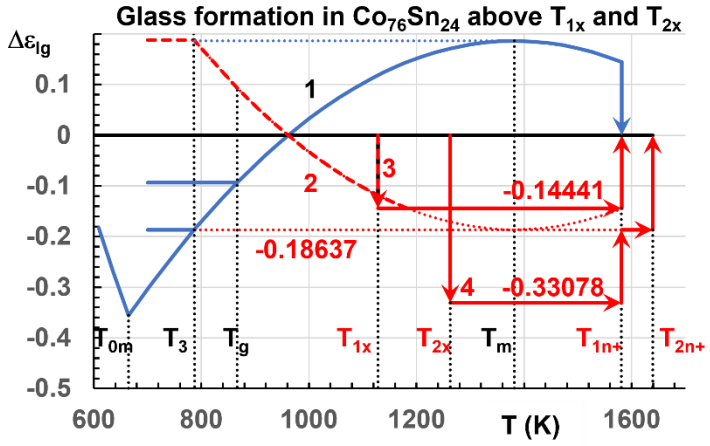


**Figure 4.** Phase 3 enthalpy coefficients above the temperatures $T_{1x}$ and $T_{2x}$. $T_{1x}$= 1263 K, $T_{2x}$= 1382 K, $T_{1n+}$= 1581.6 and $T_{2n+}$=1639.6 K. Lines 1 and 2 calculated with equations (26,29) in the absence of transition at Tx. Glassy state of 33.078% of the melt up to 1581.6 K and 18.637% from 1581.6 to 1639.6 K. Lines 1 and 2 without transition at Tx corresponding to 14.441% of glassy Phase 3.

### *4.4. Melting temperatures of $Bi_2Te_3$ and its alloys above $T_m$= 864 K*

Liquid-liquid structure transitions in metallic melts have an impact on solidification [96] and play an important role in the final microstructure and the properties of the solid alloys. We note that the compound $Bi_2Te_3$ is used for the most of Peltier cooling devices and thermoelectric generators. In alloys based on this compound, during the first heating process, a temperature-induced liquid–liquid structural transition existed at a temperature that we call $T_{1n+}$ which disappeared in the resistivity measurements by cooling from higher temperatures than $T_{n+}$ [44,45]. Solidifying at various cooling rates in these conditions, the microstructures were refined, and the hardness increased with cooling rate. The glass transition temperature of $Bi_2Te_3$ and its alloys were unknown. Applying (23) to this compound with $T_m$= 864 K and $T_{1n+}$= 967.8 K [97], the two glass transition temperatures are predicted at $\theta_g$= -0.29576 ($T_g$= 586 K) and $\theta'_g$= 0.29576 ($T'_g$= 1132 K). The presence of nucleation and recalescence temperatures and a temperature of recalescence below $T_m$ upon cooling was dependent on cooling rate. The exothermic transition at $T_{n+}$ was also observed by DSC during cooling at 135 K/min.

The equations (30,31,32) used to predict Phase 3 enthalpy increasing with temperature are determined with $\theta_g$= -0.29576 ($T_g$ = 586 K) and (9,10,12,13):

$$\varepsilon_{ls} = 1.68981(1 - \theta^2/0.23296), \quad (30)$$

$$\varepsilon_{gs} = 1.53472(1 - \theta^2/0.31736), \quad (31)$$

$$\Delta\varepsilon_{lg}(\theta) = [\varepsilon_{ls} - \varepsilon_{gs}] = [0.15509 - 2.4179 \times \theta^2]. \quad (32)$$

The singular values of the enthalpy coefficient $\Delta\varepsilon_{lg}$ ($\theta$) are: $\Delta\varepsilon_{lg}$ ($\theta_g$) = -$\Delta\varepsilon_{lg0}$ /2= -0.15509/2, -$\Delta\varepsilon_{lg}$ ($\theta_{n+}$) = -0.12017, -$\Delta\varepsilon_{lg0}$= -0.15509, $\Delta\varepsilon_{lg}$ ($\theta_{0m}$) = -0.40818. The first-order transition for $\Delta\varepsilon$= 0.40818 does not exist because it would lead to a second melting temperature higher the second glass transition $T'_g$ at 1897.1 K. It is replaced by a first-order transition with $\Delta\varepsilon$= 0.12017+0.15509= 0.27527. Two first-order transition temperatures are expected for $\theta_{n+}$= $\Delta\varepsilon$= 0.12017) and $\theta_{n+}$= $\Delta\varepsilon$= 0.27527.

The equations (33,34,35) used to predict Phase 3 enthalpy decreasing with temperature are determined with $\theta_g$= 0.29576 ($T_g$ = 1132 K) and (9,10,12,13).

$$\varepsilon_{ls} = 2.31019(1 + \theta^2/0.31848) \quad (33)$$

$$\varepsilon_{gs} = 2.46528(1 - \theta^2/0.5098), \quad (34)$$

$$\Delta\varepsilon_{lg}(\theta) = [\varepsilon_{ls} - \varepsilon_{gs}] = [-0.15509 + 2.4179 \times \theta^2]. \quad (35)$$

Lines 1 and 2 determined by (32) and (35) in Figure 5 obtained by heating from the glassy state, depend on thermal history and heating rate and lead to exothermic and endothermic transitions at $T_{1n+}$= 967.8 K.

The crystallization of Phase 3 by heating from the glassy state is predicted at $T_x$= 802 K using (14) with $\Delta\varepsilon$= 0.12017+0.15509= 0.27527, $\varepsilon_{ls0}$= 1.53472, and $\theta_{0g}^2$= 0.31736 and lead to the negative enthalpy coefficient, -0.27527, as shown in Figure 5. This transition at 802 K was observed by supercooling at 135 K/min [ (97)] and was viewed as the nucleation temperature of nanocrystals. The glassy enthalpy -0.27527×$H_m$ would be recovered at the second melting temperatures $T_{n+}$= 967.9 K ($\theta_{n+}$= 0.12017) and 998 K ($\theta_{n+}$= 0.15509). The melting enthalpy of the crystallized part would be (1-0.27527) $H_m$ = 0.72473×$H_m$ while the crystallization enthalpy would be -0.72473×$H_m$.

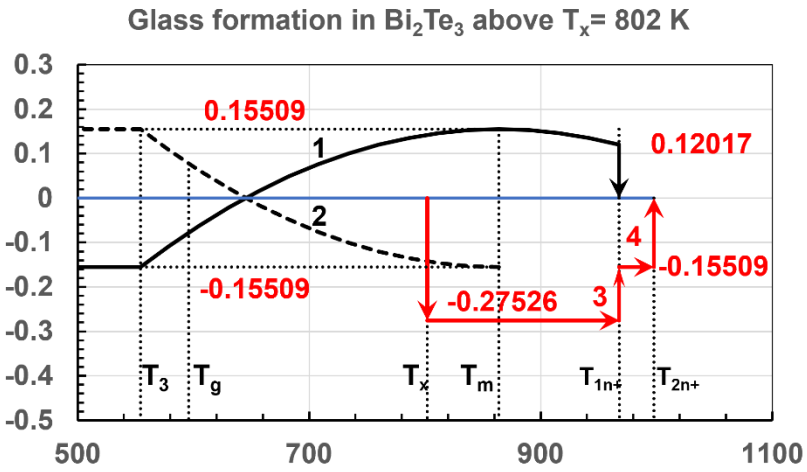


**Figure 5.** Phase 3 enthalpy coefficients above the temperature $T_x$. $T_x$= 802 K, $T_m$ = 864 K, $T_{AB}$ = 874.4 K, $T_{n+}$ = 967.9 and 998 K. Lines 1 and 2 in the absence of transition at $T_x$. Glassy state of 27.527% of the melt up to 967.9 K and 15.509% from 967.9 to 998 K. Lines 1 and 2 without transition at $T_x$ corresponding to 12.017% of glassy Phase 3.

### *4.5. The six melting temperatures of $Zr_{46}Cu_{46}Al_8$ above 1200 K*

The glass transition temperature of $Zr_{46}Cu_{46}Al_8$ is $T_g$= 715 K. There are three melting temperatures 962 K, 1034 K and 1125 K as shown in Figure 6 inducing three unknown Phases 3 observed with heating rates between 0.1666 and 2 K/s in this non-congruent alloy and three theoretical virtual glass transition temperatures equal to 1209 K, 1353 K, and 1535 K respectively [98]. Consequently, there are different coefficients $\varepsilon_{ls0}$, $\varepsilon_{gs0}$, $\theta_{0g}^2$, $\theta_{0m}^2$, $\Delta\varepsilon_{lg}$ ($\theta_{0m}$), $\Delta\varepsilon$= $\theta_{n+}$ for every one of them given in Table 1 and calculated with (9, 10, 12, 13, 15), a= 1 and $\theta_g$= -0.25676 for $T_m$ =962 K, -0.30851 for $T_m$ = 1034 K and -0.36444 for $T_m$ = 1125 K. The main phase having the highest melting enthalpy corresponds to $T_m$ =1125 K.

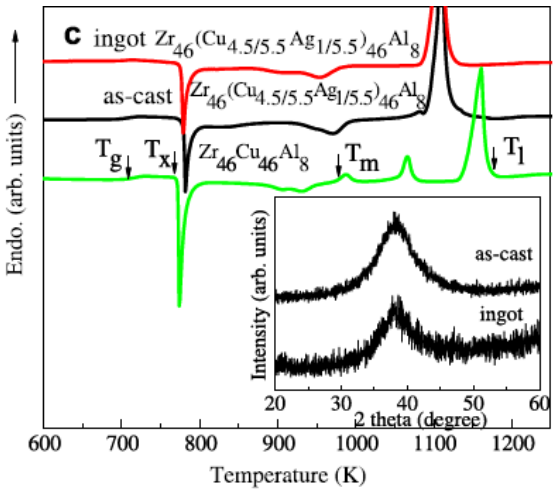


**Figure 6.** DSC of $Zr_{46}Cu_{46}Al_8$ in green around the melting temperatures using heating rates between 0.166 and 2 K/s. Reproduced with permission from [98] "XRD patterns and DSC curves of the arc-melted $Zr_{46}(Cu_{4.5/5.5}Ag_{1/5.5})_{46}Al_8$ ingot and as-cast $Zr_{46}(Cu_{4.5/5.5}Ag_{1/5.5})_{46}Al_8$ BMG sample, together with DSC curve of as-cast $Zr_{46}Cu_{46}Al_8$ BMG alloy". Melting temperatures of 3 phases in $Zr_{46}Cu_{46}Al_8$: 962 K, 1034 K and 1125 K. Copyright 2008 Elsevier.

**Table 1.** Multiple melting temperatures $T_m$ and $T_{n+}$ of $Cu_{46}Zr_{46}Al_8$. $T_g$ = 715 K; $T_m$, the first melting temperature; $\theta_g$, the reduced glass transition temperature; $\varepsilon_{ls0}$, $\theta_{0m}^2$, $\varepsilon_{gs0}$, $\theta_{0g}^2$ calculated with (9,10,12,13); $\Delta\varepsilon_{lg}$ ($\theta_{0m}$) with (15), the enthalpy coefficient of Phase 3 at $\theta = \theta_{0m}$; $\Delta\varepsilon = \theta_{n+}$ the enthalpy coefficient singular values of glassy Phase 3 above $T_x$ = 763 K; $T_{n+}$ (K), the theoretical second melting temperatures; Obs., with yes when $T_{n+}$ has been observed in Figure 7; $T'_g$, the virtual glass transition temperature above $T_{n+}$.

| $T_g$ | $T_m$ | $\theta_g$ | $\varepsilon_{ls0}$ | $\theta_{0m}^2$ | $\varepsilon_{gs0}$ | $\theta_{0g}^2$ | $\Delta\varepsilon_{lg}$ ($\theta_{0m}$) | $\Delta\varepsilon = \theta_{n+}$ | $T_{n+}$ | Obs. | $T'_g$ |
|---|---|---|---|---|---|---|---|---|---|---|---|
| 715 | 962 | -025676 | 1.74324 | 0.19893 | 1.61486 | 0.27642 | -0.4527 | 0.06419 | | | 1209 |
| 715 | 962 | -0.25676 | 1.74324 | 0.19893 | 1.61486 | 0.27642 | -0.4527 | 0.09947 | 1057 | | 1209 |
| 715 | 962 | -0.25676 | 1.74324 | 0.19893 | 1.61486 | 0.27642 | -0.4527 | 0.12838 | 1086 | | 1209 |
| 715 | 962 | -0.25676 | 1.74324 | 0.19893 | 1.61486 | 0.27642 | -0.4527 | 0.22785 | 1181 | | 1209 |
| 715 | 1034 | -0.30851 | 1.69149 | 0.23193 | 1.53723 | 0.31617 | -0.40957 | 0.07713 | | | 1353 |
| 715 | 1034 | -0.30851 | 1.69149 | 0.23193 | 1.53723 | 0.31617 | -0.40957 | 0.11953 | 1158 | | 1353 |
| 715 | 1034 | -0.30851 | 1.69149 | 0.23193 | 1.53723 | 0.31617 | -0.40957 | 0.15426 | 1194 | | 1353 |
| 715 | 1034 | -0.30851 | 1.69149 | 0.23193 | 1.53723 | 0.31617 | -0.40957 | 0.19665 | 1237 | Yes | 1353 |
| 715 | 1034 | -0.30851 | 1.69149 | 0.23193 | 1.53723 | 0.31617 | -0.40957 | 0.27378 | 1317 | Yes | 1353 |
| 715 | 1125 | -0.36444 | 1.63556 | 0.26492 | 1.45333 | 0.35311 | -0.36296 | 0.09111 | | | 1535 |
| 715 | 1125 | -0.36444 | 1.63556 | 0.26492 | 1.45333 | 0.35311 | -0.36296 | 0.1412 | 1284 | Yes | 1535 |
| 715 | 1125 | -0.36444 | 1.63556 | 0.26492 | 1.45333 | 0.35311 | -0.36296 | 0.18222 | 1330 | Yes | 1535 |
| 715 | 1125 | -0.36444 | 1.63556 | 0.26492 | 1.45333 | 0.35311 | -0.36296 | 0.32342 | 1489 | Yes | 1535 |
| 715 | 1125 | -0.36444 | 1.63556 | 0.26492 | 1.45333 | 0.35311 | -0.36296 | 0.36296 | 1533 | Yes | 1535 |

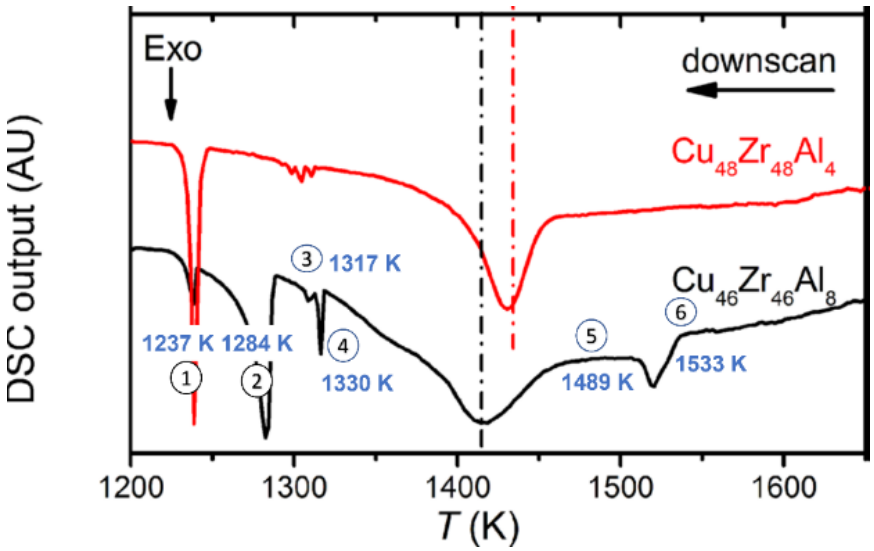


**Figure 7.** Melt phase transitions in $Cu_{46}Zr_{46}Al_8$ above 1200 K. Reproduced with permission from [41]. "Melt phase transitions in $Cu_{48}Zr_{48}Al_4$ and $Cu_{46}Zr_{46}Al_8$. The DSC upon cooling for $Cu_{48}Zr_{48}Al_4$ (red one) and $Cu_{46}Zr_{46}Al_8$ (black one) melts in arbitrary unit (AU) upon cooling from 1623 K with a 0.167 K/s rate". Copyright 2014 American Physical Society. Peaks numbered 1 to 6 for $Cu_{46}Zr_{46}Al_8$ with predicted temperatures $T_{n+}$: for $T_m$= 1125 K (N°2-1284K, N°4-1330 K, N°5- 1489 K, N°6- 1533 K); for $T_m$= 1034 K (N°1- 1237 K, N°3- 1317 K) and for $T_m$= 962 K, no temperature $T_{n+}$ above 1200 K. Copyright 2013 AIP Publishing.

Six first-order transition temperatures accompanied by exothermic latent heats were observed above 1200 K by cooling the melt from 1650 K as shown in Figure 7 [41]. These temperatures predicted in Table 1 are melting temperatures upon heating. Peaks numbered 1 to 6 correspond to predicted temperatures $T_{n+}$: for $T_m$= 1125 K (N°2-1284K, N°4-1330 K, N°5- 1489 K, N°6- 1533 K); for $T_m$= 1034 K (N°1- 1237 K, N°3- 1317 K) and for $T_m$= 962 K, no $T_{n+}$ above 1200 K. Peaks N°s1 and 3 are weak compared to N°s 2, 4, 5 and 6. The sum of predicted enthalpy coefficients of peaks N°s2, 4, 5 and 6 is equal to -0.1412-0.18222-0.32342-0.36293= -1.0098≅ -1 below $T_{1n+}$= 1284 K instead of $T_m$ = 1125 K in good agreement with the melting of a glass having an enthalpy coefficient equal to -1, the enthalpy coefficient of full crystallization. A full glassy state exists below $T_{1n+}$= 1284 K and then, the glassy state fraction declines with three increases of $T_{n+}$ from $T_{1n+}$ to $T_{4n+}$= 1533 K.

All transitions of Phases 3 with $T_m$= 1125 K are represented in Figure 8. Lines 1 and 2 represent Eqs. (15,16). The transition at $T_x$ = 760.3 K occurs when $\Delta\varepsilon_{lg}$ = 0 for the phase 3 enthalpy coefficient corresponding to the lowest melting temperature $T_m$= 962 K. The formation, by heating, of a glass phase having an enthalpy equal to that of crystals, occurs using heating rates inducing a first-order transition at $T_x$ without crystallized fraction. The observation of glass fractions melting above $T_m$ could be obtained by heating because all first-order transitions at $T_{n+}$ were reversible and corresponded to singular enthalpies of the glassy phase and probably various percolation thresholds [41]. The first-order transition at $T_x$= 760.3 K leading to a glassy fraction equal to 100 % corresponds to $\Delta\varepsilon$= -1 at a temperature far below $T_m$ = 1125 K using a low heating rate. Nevertheless, a crystallization enthalpy occurs at $T_m$ = 1125 K as shown in Figure 6 because the melt, in this case, has not been overheated above $T_{4n+}$= 1533 K before cooling [98]. The glassy state obtained at $T_x$= 760.3 K could totally escape crystallization following the red broken line N°3 using low heating rates such as 0.333 K/s if the melt is previously overheated above $T'_g$= 1535 K before cooling as shown in Figure 7.

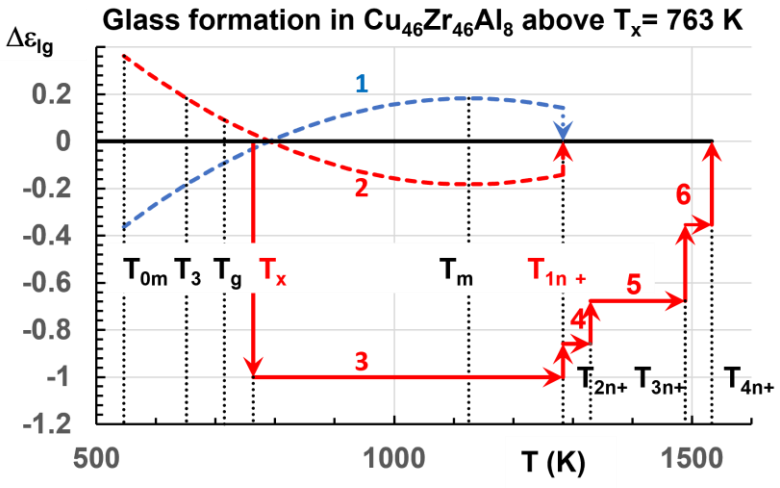


**Figure 8.** Multiple transitions and glassy states expected in the melt fraction with $T_m$= 1125 K of $Cu_{46}Zr_{46}Al_8$. Eq. (15,16) represented by Lines 1 and 2 using enthalpy coefficients given in Table 1 for $T_m$= 1125 K. Glass states of Phases 3 noted 3, 4, 5, and 6. $T_{0m}$= 545.9; $T_3$= 651.6 K; $T_g$= 715 K; $T_x$= 760.3 K; $T_m$= 1125 K; $T_{1n+}$ = 1283.9; $T_{2n+}$= 1330 K; $T_{3n+}$= 1488.8 K; $T_{4n+}$= 1533.3 K. The reversible red broken Line N°3 observed above 1200 K with cooling and heating rates of 0.333 K/s in Figure 7.

The first order transitions are due to liquid super atom formation at $T_{n+}$. Observations of multiple temperatures $T_{n+}$ are facilitated in this alloy because they have a first-order character much stronger than those observed in $La_{50}Al_{35}Ni_{15}$ and $Pd_{42.5}Ni_{42.5}$ $P_{15}$ studied by [37,38] due, here, to the spontaneous formation and percolation of solid super atoms instead of having bonds progressively built-in liquid super atoms (clusters-bound colloids) during slow cooling [77].

## 5. Conclusions

This paper is devoted to liquid-liquid transitions in glass-forming melts. A first liquid-liquid transition was often observed at a temperature $T_{1n+}$ above the equilibrium thermodynamic transition $T_m$ after heating from the glassy state without previous first-order transition at a temperature $T_x$ weaker than $T_m$. This transition at $T_{n+}$ was exothermic or endothermic and associated with antibonds or bonds breaking predicted by the non-classical nucleation model and in agreement with the configuron percolation model as already shown in previous publications.

Separation phenomena were observed by molecular dynamics simulations of monoatomic liquid elements at very high heating rates and still predicted. Full melting of Ag, Cu, Zr and Fe were obtained at temperatures much higher than $T_m$ showing that the crystal fraction can fully profit from the disappearance of any glass phase above $T_m$. An increase in the melting temperature of glassy phases at high heating rate is due to finite mobility of configurons – broken chemical bonds, which at relatively low heating rates quickly condense causing the typical first-order phase transformation arrest at the temperature $T_x$. At higher heating rates however, there is not enough time for condensation to occur and thus the melting occurs at a much higher temperature when the percolation via configurons occurs.

In this paper, some mysterious aspects of the first-order transition occurring at $T_x$ and leading to crystallization were enlightened, considering phase separation between a glassy fraction having a glass transition temperature higher than $T_m$ and a second fraction, crystallizing at $T_x$, and melting at $T_m$. The non-classical nucleation model predicts the existence of two glassy phases at $T_g$ and $T'_g$ in two different temperature domains separated by the temperature $T_x$. The transition at $T_x$ increases $T_g$ up to $T_x$ and induces a new glassy

phase above $T_x$. The temperature $T'_g$ is virtual because the glass phase has a melting temperature higher than $T_m$ and lower than $T'_g$.

These new melting temperatures are observable at $T_{n+}$ at low heating rates as already anticipated by the reduction of the crystallization enthalpy of some monoatomic elements after supercooling and recalescence. Several new examples were found in publications. Three liquid-liquid transitions in bismuth observed in two different experiments lead to a total glassy fraction of 86.7% and a melting temperature equal to $1.867T_m$ in one of the two experiments and to $1.438T_m$ in the other. Four reversible first-order liquid-liquid transitions in $Cu_{46}Zr_{46}Al_8$ lead to a glassy fraction of 100 %, for the phase with $T_m$= 1125 K and a melting temperature of $1.36T_m$. Predictions of complementary liquid-liquid transitions were made for $Co_{76}Sn_{24}$, $Pd_{40}Ni_{40}P_{20}$, and $Bi_2Te_3$ beyond the first liquid-liquid transitions already observed.

The first-order transitions at $T_x$ observed by heating were accompanied by latent heats composed of singular values of the glass enthalpy or of their sum as already shown for monoatomic elements. They determined the first-order liquid-liquid transitions at $T_{n+}$ above $T_m$ which were reversible in $Cu_{46}Zr_{46}Al_8$ and observed with the same latent heats by cooling from homogeneous liquid state and heating due the melting and formation of percolating solid superclusters (superatoms)respectively. The same transitions at $T_{n+}$ observed in $La_{50}Al_{35}Ni_{15}$ and $Pd_{42.5}Ni_{42.5}$ $P_{15}$ involve much weaker latent heats by cooling because percolating liquid superclusters (superatoms) formed at $T_{n+}$ from homogeneous liquid are progressively solidified by cooling from $T_{n+}$ instead of being fully solidified at $T_{n+}$.

The melts are rejuvenated above $T'_g = 2T_m - T_g$ because all growth nuclei of crystals are eliminated by superheating above $T'_g$. Many techniques of quenching, used up to now, to escape crystallization, do not overheat melts far above $T_m$ before quenching and are not able to reveal the various glassy states above $T_x$.

**Author Contributions:** Conceptualization, RFT; methodology, RFT; investigation and formal analysis, RFT and MIO; data curation, RFT; writing—original draft preparation, RFT; writing—review and editing, RFT and MIO; All authors have read and agreed to the published version of the manuscript."

**Funding:** This research received no external funding.

**Data Availability Statement:** Data are reported within the paper.

**Acknowledgments:** In this section, you can acknowledge any support given which is not covered by the author contribution or funding sections.

**Conflicts of Interest:** The authors declare no conflict of interest.

## References


1. Poole P.H., Grande T., Sciorfino F., and Angel C.A. Amorphous polymorphism. *Comput. Mater. Sci.* **1995**, 4, 373-382.
2. Brazhkin V.V., Popova S.V., and Voloshin R.N. High pressure transformations in simple metals. **1997**, 15, 207-305.
3. Poole P.H., Grande T., Angell C.A., and McMillan P.F. Polymorphic phase transitions in liquids and glasses. *Science.* 1**997,** 275, 322.
4. Mishima O., and Stanley H.F. The relationship between liquid, supercooled and glassy water. **1998**, 396, 329-335.
5. Stillinger F.H., and Debenedetti P.G. Supercooled liquids and the glass transition. *Nature.* **2001**, 410, 259-267.
6. Angilella G.N., Leys F.E., March N.H., and Pucci R. Phase transitions in liquids and glasses. **2003**, 41, 211-226.
7. Debenedetti P.G. Supercooled and glassy water. *J. Phys.: Condens. Matter.* **2003,** 15, 1669-1726.
8. McMillan P.F. Polyamorphic transformations in liquids and glasses. *J. Mater.Chem.* **2004**, 14, 1506-1512.
9. McMillan P.F., Wilson M., Wilding M.C., Daisenberger D., Mezouar M., and Greaves G.N. Polyamorphism and liquid-liquid phase transitions: Challenges for experiment and theory. **2007**, 19, 415101.
10. Berthier L., Biroli G. Theoretical perspective on the glass transition and amorphous materials. *Rev. mod. Phys.* **2011**, 83, 587.
11. Stanley H.E. Book Series: Advances in Chemical Physics. [book auth.] H.E. Stanley. *Liquid polymorphism.* s.l.: John Wiley & Sons, Inc., **2013**, Vol. 152.
12. Gallo P., Amann-Winkel K., Angell C.A., Anisimov M.A., Caupin F., Chakravarty C., Lascaris E., Loerting T., Panagiotopoulos A.Z., Russo J.,Selberg J.A., J.A. Stanley J.A.,Tanaka H. , Vega C., Xu L. , and Pettersson G.L. A tale of two liquids. *Chem. Rev.* **2016**, 116, 7463-7500.
13. Handle H., Loerting T., and Sciortino F. Supercooled and glassy water: metastable liquid(s), amorphous solid(s), and a no-man's land. **2017,** 114, 13336-13344.
14. Palmer J.C., Poole P.H., Sciorfino F., and Debenedetti P.G. Studies of liquid-liquid transition in water and water-like models. **2018,** 118, 9129-9151.
15. Tanaka H. Liquid-liquid transition and polyamorphism. *J. Chem. Phys.* **2020**, 153, 130901.
16. Kearns K.L., Swallen S.F., and Ediger M.D., Wu T., Sun Y., Yu L. Hiking down the energy landscape: Progress toward the Kauzmann temperature via vapor deposition. *J. Phys. Chem. B.* **2008**, 112, 4934-4942.
17. Kearns K.L., Swallen S.F., and Ediger M.D., Wu T. and Yu L. Influence of substrate temperature on the stability of glasses prepared by vapor deposition. *J. Chem. Phys.* **2007,** 127, 154702.
18. Leon-Gutierrez E, Sepulveda A., Garcia G., Clavaguera-Mora M.T. and Rodriguez-Vieja J. Stability of thin film glasses of toluene and ethylbenzene formed by vapor deposition: an in situ nanocalorimetric study. *Phys. Chem. Chem. Phys.* **2010,** 12, 14693-14698.
19. Ishii K., Nakayama H., Hirabayashi S., Moriyama R. Anomalously high-density glass of ethylbenzene prepared by vapor deposition at temperatures close to the glass-transition temperature. *Chem. Phys. Lett.* **2008**, 459, 109-112.
20. Ha A., Cohen I., Zhao X., Lee M., and Kivelson D. Supercooled liquids and polyamorphism,. *J. Phys. Chem. Lett.* 1996, 100, 1-4.
21. Kivelson D., Kivelson S.A., Zhao X., Nussinov Z., Tarjus G. A thermodynamic theory of supercooled liquids. *Physica A.* **1995**, 219, 27-38.
22. Miltenburg K.V. and Blok K. Calorimetric investigation of a new solid phase in Triphenylphosphite. *J. Phys. Chem.* **1996**, 100, 16457-16459.
23. Kurita R., and Tanaka H. On the abundance and general nature of the liquid-liquid phase transition in molecular systems,. *J. Phys.: Condens. Matter.* **2005,** 17, L293-L302.
24. Zhu M., Wang J-Q, Perepezko J.H., and Yu L. Possible existence of two amorphous phases of D-Mannitol related by a first-order transition. *J. Chem. Phys.* **2015**, 142, 244504.
25. Kobayashi, K. and Tanaka H. The reversibility and first-order nature of liquid-liquid transition in a molecular liquid,. *Nature Comm.* **2016**, 7, 13438.
26. An Q. Johnson W.L., Samwer K., Corona S.L., Goddart III W.A. Formation of two glass phases in binary Cu-Ag liquid. *Acta Mater.* **2020**, 195, 274-281.
27. An Q. Johnson W.L., Samwer K., Corona S.L., and Goddard III W. A. First-order transition in liquid Ag to the heterogeneous G-Phase. *J. Phys. Chem. Lett.* **2020**, 11, 632-645.
28. Bazlov A.I., Louzguine-Luzguin D.V. Crystallization of FCC and BCC liquid metals studied by molecular dynamics simulation. *Metals.* **2020**, 10, 1532.
29. Becker S., Devijver E., Molinier R., and Jakse. N. Glass-forming ability of elemental zirconium. *Phys. Rev. B.* **2020**, 102, 104205.
30. Popel P.S., Sidorov V.E. Microheterogeneity of liquid metallic solutions and its influence on the structure and propertes of rapidly quenched alloys. *Mater.Sci. Eng.* 1997, A 226-2289, 237-244.
31. Kim Y.H., Kiraga K., Inoue A., Masumoto T., and Jo H.H. Crystallization and high mechanical strengthof Al-based amorphous alloys. *Materials Trans.* **1994**, 35, 293-302.
32. Hu Q., Sheng H.C., Fu M.W., Zeng X.R. Influence of melt temperature on the Invar effect in (Fe71.2B.024Y4.8)96Nb4 bulk metallic glasses. *J. Mater. Sci.* **2019**, 48, 6900-6906.

33. 33. Jiang H-R, Bochtler B., Riegler X.-S. , Wei S.S., Neuber N., Frey, M., Gallino I., Busch R., Shen J. Thermodynamic and kinetic studies of the Cu-Zr-Al(-Sn) bulk metallic glasses. *J. All. Comp.* **2020,** 844, 156126.
34. 34. Yue Y. Experimental evidence for the existence of an ordered structure in a silicate liquid above its liquidus temperature. *J. Non-Cryst. Sol.* 2004, 345 & 346, 523-527.
35. 35. Wei S., Yang F., Bednarcik J., Kaban I., Shuleshova O., Meyer A. & Busch R. Liquid-liquid transition in a strong bulk metallic glass-forming liquid. *Nature Commun.* **2013**, 4, 2083.
36. 36. C. Way, P. Wadhwa, R. Busch. The influence of shear rate and temperature on the viscosity and fragility of the Zr41.2Ti13.8Cu12.5Ni10.0Be22.5 metallic-glass-forming liquid. *Acta Materialia.* **2007**, 55, 2977-2983.
37. 37. Chen E.-Y., Peng S.-X., Peng, Michiel M.D., Vaughan G.B.M., Yu Y., Yu H.-B., Ruta B., Wei S., Liu L. Glass-forming ability correlated with the liquid-liquid transition in Pd42.5Ni42.5P15 alloy. *Scripta Materialia.* 2021, 193, 117-121.
38. 38. Xu W., Sandor M.T., Yu Y., Ke H.-B., Zhang H.P., Li M.-Z, Wang W.-H., Liu L. & Wu Y. Evidence of liquid-liquid transition in glass-forming La50Al35Ni15 melt above liquidus temperature. *Nat. Commun.* **2015**, 6, 7696.
39. 39. Wang L., Bian X., Liu J. Discontinuous structural phase transition of liquid metal and alloys. *Phys. Lett. A.* **2004**, 326, 429-435.
40. 40. Y. Greenberg, E. Yahel, E.N. Caspi, C. Benmore, B. Beuneu, M.P. Daniel, and G. Markov. Evidence for a temperature-driven structural transition in liquid bismuth. *EPL.* **2009**, 86, 36004.
41. 41. Zhou C., Hu L.,Sun Q., Qin J., Brian X., and Yue Y. Indication of liquid-liquid phase transition in CuZr-based melts. *Appl. phys. Lett.* **2013**, 103, 171904.
42. 42. Tanaka H. Bond orientational order in liquids: Towards a unified description of water-like anomalies, liquid-liquid transition, glass transition, and crystallization. *Europ. Phys. J.* **2012**, 35, 113.
43. 43. He Y-X., Li J., Wang J., Kou H., Beaugnon E. Liquid-liquid structure transition and nucleation in undercooled Co-B eutectic alloys. *Applied Physics A.* **2017**, 123, 391.
44. 44. Yu Y., Wu Z., Cojocaru-Morédin O., Zhu B., Wang X.-Y., Gao N., Zhuang -Y., Zu F.-Q. Dependence of solidification for Bi2Te3-xSex alloys on their liquid states. *Scient. Rep.* **2017**, 7, 2463.
45. 45. Yu Y., Lv L., Wang X.-Y., Zhu B., Huang Z.-Y., Zu F.-Q. Influence of melt overheating treatment on solidification behavior of BiTe-based alloys at different cooling rates. **2015**, 88, 743-750.
46. 46. Tournier R.F., and Beaugnon E. Texturing by cooling a metallic melt in a magnetic field. *Sci. Technol. Adv. Mater.* **2009**, 10, 014501.
47. 47. Legrand B .A., Chataigner D., Perrier de la Bathie R., and Tournier R.F. Orientation by solidification in a magnetic field. A new processto texture SmCo compounds used as perrmanent magnets. *J. Magn. Magn. Mater.* **1997**, 173, 20.
48. 48. Turnbull D. Kinetics of solidification of supercooled liquid mercury. *J. Chem. Phys.* **1952**, 20, 411.
49. 49. Kelton K.F. Crystal nucleation in liquids and glasses. *Sol. State Phys.* **1991**, 45, 75-177.
50. Tournier R. F. Presence of intrinsic growth nuclei in overheated and undercooled liquid elements. *Physica B.* **2007**, 392, 79-91.
51. Tournier R.F. Lindemann's rule applied to the melting of crystals and ultra-stable glasses. *Chem. Phys. Lett.* **2016,** 651, 198-202. Erratum in **2017**, 675, 174.
52. 52. —. Thermodynamic origin of the vitreous transition. *Materials.* **2011**, 4, 869-892.
53. 53. —. Thermodynamic and kinetic origin of the vitreous transition. *Intermetallics.* **2012**, 30, 104-110.
54. 54. —. Fragile-to-fragile liquid transition at Tg and stable-glass phase nucleation rate maximum at the Kauzmann temperature. *Physica B,* **2014**, 454, 253-271.
55. 55. Tournier R. F. Glass phase and other multiple liquid-to-liquid transitions resulting from two-liquid competition. *Chem. Phys. Lett.* **2016**, 665, 64-70.
56. 56. Tournier R.F. Crystallization of supercooled liquid elements induced by superclusters containing magic atom numbers. *Metals.* **2014**, 4, 359-387.
57. 57. Franck F.C. Supercooling of liquids. *Proc. Roy. Soc. Lond.* **1952**, A215, 43-46.
58. 58. Tournier R.F. Homogeneous nucleation of phase transformations in supercooled water. *Physica B.* 2020, Vol. 579, p. 411895.
59. 59. —. Amorphous ices. [ed.] Pascal Richet. *Encyclopedia of Glass Science, Technology, History, and Culture.* Hoboken: Wiley & Sons, **2021**, 1, 3.14.
60. 60. Oguni M., Maruyama S., Wakabayashi K., Nagoe A. Glass transitions of ordinary and heavy water within silica-gel nanopores, *Chem. Asian J.* **2007**, 2, 4, 514-520.
61. 61. Speedy R.J. and Angell C.A. Isothermal compressibility of supercooled water and evidence for a thermodynamic singularity at -45°C. *J. Chem. Phys.* **1976**, 65, 851-858.
62. 62. Tournier R. F., and Ojovan M. I. Dewetting Temperatures of Prefrozen and Grafted Layers in Ultrathin Films Viewed as Melt-Memory Effects. *Physica b.* **2021**, 611, 412796.
63. 63. Takaiwa D., Atano I., Koga K., and Tanaka H.,. Phase diagram of water in carbon nanotubes. *PNAS.* **2008,** 105 (1), 39-43.
64. 64. Assland S. and McMillan P.F. Density-driven liquid-liquid phase separation with system Al2O3-Y2O3. *Nature.* **1994**, 369, 633-636.
65. 65. Tournier R.F. First-order transitions in glasses and melts induced by solid superclusters nucleated by homogeneous nucleation instead of surface melting. *Chem. Phys.* **2019**, 524, 40-54.

66. 66. Hassaine M., Jimenez-Rioboo R.J., Sharapova I.V., Korolynk O.A., Krivchikov A.I., and Ramos M.A. Thermal properties and Brillouin -scattering study of glass, crystal, and "glacial" states in n-butanol. *J. Chem. Phys.* **2009**, 131, 174508.
67. 67. Krivchikov A.I., Hassaine M., Sharapova I.V., Korolyuk O.A., Jimenez-Rioboo R.J., Ramos M.A. Low temperature properties of glassy and crystalline states of n-butanol. *J. Non-Cryst. Sol.* **2011**, 357, 524-529.
68. 68. Hays C.C. and Johnson W.L. Undercooling of bulk metallic glasses processed by electrostatic levitation. *J. Non-Cryst. Sol.* **1999**, 250-252, 596-600.
69. 69. B. Yang, J.H. Perepezko, J.W.P. Schmelzer, Y. GaO, and C. Schick. Dependence of crystal nucleation on prior liquid overheating by differential fast scanning calorimeter. *J. Chem. Phys.* **2014**, 140, 104513.
70. 70. Ojovan M.I. Glass formation in amorphous SiO2 as a percolation phase transition in a system of network defects. *J. Exp. Theor. Phys. Lett;.* **2004**, 79 (12), 632-634.
71. 71. —. Topological characteristics of bonds in SiO2 and GeO. oxide systems at glass-liquid transition. *J. Exp. Theor. Phys.* **2006**, 103 (5), 819-829.
72. 72. —. Ordering and structural changes at the glass-liquid transition. *J. Non-Cryst. Sol.* **2013,** 382, 79.
73. 73. —. Viscous flow and the viscosity of melts and glasses. *Phys. Chem. Glasses.* **2012**, 53, 143-150.
74. 74. Sanditov D.S., Ojovan M.I. On relaxation nature of glass transition in amorphous materials. *Physica B.* **2017**, 523, 96-113.
75. 75. Ojovan M.I., Louzguine Luzgin D.V. Revealing Structural Changes at Glass Transition via Radial Distribution Functions. **2020**, 124, 3186-3194.
76. 76. Tournier R.F. and Ojovan M.I. Undercooled Phase Behind the Glass Phase with Superheated Medium-Range Order above Glass Transition Temperature. *Physica B.* **2021**, 602, 412542.
77. 77. —. Building and breaking bonds by homogenous nucleation in glass-forming melts leading to three liquid states. *Materials.* **2021**, 14, 2287.
78. 78. Tournier R.F. Validation of non-classical homogeneous nucleation model for G-glass and L-glass formations in liquid elements with recent molecular dynamics simulations. *Scripta Mater.* **2021**, 199, 113859.
79. 79. Tournier R.F. and Ojovan M.O. Prediction of Second Melting Temperatures Already Observed in Pure Elements by Molecular Dynamics Simulations. *Materials.* **2021**, 14, 6509.
80. 80. Tournier R.F. Influence of Fermi energy equalization on crystal nucleation in glass melts. *J. All. Comp.* **2009,** 483, 94-96.
81. 81. Vinet B., Magnusson L., Fredriksson H., and Desré P.J. Correlations between surface and interface energies with respect to crystal nucleation. *J. Coll. Interf. Sci.* **2002**, 255, 363-374.
82. 82. Mukherjee S., Zhou Z., Schroers J., Johnson W.L., Rhim W.K. Overheating threshold and its effect on time-temperature-transformation diagrams of zirconium based bulk metallic glasses. *Appl. Phys. Lett.* **2004**, 84 (24), 5010-5012.
83. 83. Wang J., Li J., Hu R., Kou H., Beaugnon E. Evidence for the structure transition in a liquid Co-Sn alloy by in-situ magnetization measurement. *Mater. Lett.* **2015**, 145, 261-263.
84. 84. He Y., Li J., Li L., Wang J., Yildiz E., Beaugnon E. Composition dependent characteristic transition temperatures o Co-B melts. *J. Non-Cryst. Sol.* **2019**, 522, 119583.
85. 85. Wang J., He Y., Li J., Li C., Kou H., Zhang P., Beaugnon E. Nucleation of supercooled Co melts under a high magnetic field. *Mater. Chem. Phys.* **2019**, 225, 133-136.
86. 86. Bian X.F., Sun B.A., Hu L.N., Jia Y.B. Fragility of superheated melts and glass-forming ability in Al-based alloys. *Phys. Lett. A.* **2005**, 335, 61-67.
87. 87. Lan S., Ren Y., Wei X.Y., Wang B., Gilbert E.P., Shibayama T., Watanabe S., Ohnuma M., & Wang X.-L. Hidden amorphous phase and reentrant supercooled liquid in Pd-Ni-P metallic glass. *Nat. Commun.* **2017,** 8, 14679.
88. 88. Tournier R.F. and Ojovan M.I. Comments about a recent publication entitled entitled "Improving glass forming ability of off-eutectic metallic glass formers by manipulating primary crystallization reactions". *Scripta Mater.* june 12 2021, **2021**, Vol. under publication.
89. 89. Zeng Y.Q., Yu J.S.,Tian Y., Hirata A., Fujita T., Zhang X.H., Nishiyama N., Kato H., Jiang J.Q., Inoue A., Chen M.W. Response to the commentary by Robert Tournier and Michael Ojovan on our publication entitled "Improving glass forming. *Scripta Mater.* june13, **2021**, Vol. under publication.
90. 90. Adams G., Gibbs J.H. On the temperatutre dependence of cooperative relaxation properties in glass-forming liquids. *J. Chem. Phys.* **1965,** 43, 139.
91. 91. C.-Y. Liu, J. He, R. Keunings, C. Bailly. new linearized relation for the universal viscosity-temperature behavior of polymer melts. *Macromolecules.* **2006**, 39, 8867-8869.
92. 92. Vopson M.M., Rugers N., Hepburn I. The generalized Lindemann Melting coefficient. *Sol. State Commun.* **2020**, 318, 113977.
93. 93. Jiang J., Saksl K., Nishiyama N., Inoue A. Crystallization in Pd40N0P20 glass. *J. Appl. Phys.* **2002**, 92 (7), 3651-3656.
94. Wilde G., Görler G.P., Willnecker R., Dietz G. The thermodynamic properties of Pd40Ni40P20 in the glassy, liquid, and crystalline states. *Appl. Phys. Lett.* **1994**, 65(4), 397-399.
95. Qiu X., Li J., Wang J. , Guo T., Kou H., Beaugnon E.,. Effect of liquid-liquid structure transition on the nucleation in undercooled Co-Sn eutectic alloy. *Mater.Chem. and Phys.* **2016**, 170, 261-265.

96. He Y.-X., Li J.-S, Wang J., Beaugnon E. Liquid-liquid structure transition in metallic melt and its impact on solidification: a review. [ed.] Elsevier. *Trans. Nonferr. Met. Soc. China.* **2020**, 30 (9), 2293-2310.
97. Connel L.C., Pokhrel N., Logan M., Voss C., Buna D. Thermal characterization of semi-conductor Bi2Te3 alloys using differential calorimetry. *engphys-bunabi2te3.* [Online]
98. Jian Q.K., Wang X.D., Nie X.P., Zhang G.Q., Ma H., Fecht H.J., Bendnarck J., Franz H., Liu Y.G., Cao Q.P., Jiang J.Z. Zr-(Cu,Ag)-Al bulk metallic glasses. *Acta Mater.* **2008**, 56, 1785-1796.